Dip Coating of Water-Resistant PEDOT:PSS Films Based on Physical Crosslinking

Shunsuke Yamamoto[*a], *Ryusei Miyako*[a], *Ryota Maeda*[a], *Yuya Ishizaki*[ab], *Masaya Mitsuishi*[a]

AUTHOR ADDRESSES

[a] *Graduate School of Engineering, Tohoku University, 6-6-11 Aramaki, Aoba, Sendai 9808579, Japan*

[b] *Department of Chemistry, College of Science, Rikkyo University, 3-34-1, Nishi-Ikebukuro, Toshima, Tokyo 171–8501, Japan*

KEYWORDS

Organic Mixed Conductors, Dip Coating, Conductive Polymers, Organic Electrochemical Transistors

ABSTRACT

Water-resistant poly(3,4-ethylenedioxythiophene):poly(styrene sulfonate) (PEDOT:PSS) films are valuable in biomedical applications; however, they typically require crosslinkers to stabilize the films, which can introduce undesired aggregation or phase separation reactions. Herein, we developed a dipping-based processes to prepare PEDOT:PSS films on non-planar surfaces without crosslinker. Sequential soaking of a dip-coated PEDOT:PSS film in ethanol and water imparted water resistance to the film. Microscopic and spectroscopic techniques were used to monitor the process and confirmed that the ethanol soaking eluted the excess PSS from the film bulk, which stabilized the film prior to the water-soaking process. The obtained films acted as conductors and semiconductors on curved surfaces, including three-dimensional (3D)-printed objects. A film deposited on a curved surface was successfully applied as the channel layer in a neuromorphic organic electrochemical transistor. This approach will enable integrated bioelectronic and neuromorphic applications that can be readily deployed for facile prototyping.

TEXT

1. Introduction

Organic mixed ion–electron conductors (OMIECs) have attracted considerable interest in electronics and material science fields.[1-2] OMIEC materials transport both ions and electrons (holes); therefore, these materials are desirable for transducing ionic and electronic signals, particularly in biological applications. Bioelectronics is an emerging field that promises improved healthcare monitoring, point-of-care testing, and advanced medical care.[3-7] Biosensing employs various sensing components such as bioelectrodes[8-11] and organic electrochemical transistors (OECTs).[12,13] A remarkable feature of these devices is that they can operate in aqueous environments, providing significant benefits to medical implant applications. Several previous studies have successfully used these devices to monitor heartbeat, brain activity, and electrophysiology in real time.[14-16]

An important aspect of aqueous operation is the stability of the film, and the dissolution or delamination of OMIEC films must be avoided. Owing to the nature of OMIECs, the ion transport moieties are located in the hydrophilic part basically. For example, in the well-known mixed conductor poly(3,4-ethylenedioxythiophene):poly(styrene sulfonate) (PEDOT:PSS), the sulfonate ($-SO_3^-$) groups on the PSS act as ion-transporting moieties, which stabilize the colloidal particles in commercially available PEDOT:PSS water dispersions.[17-19] Crosslinkers are commonly used to stabilize these films against dissolution and delamination of the films by a chemical reaction. Various types of crosslinkers have been proposed for PEDOT:PSS, such as (3-glycidyloxypropyl)trimethoxysilane (GOPS),[20,21] divinyl sulfone (DVS),[22,23] and polyethylene glycol diglycidyl ether (PEGDE).[24-26] To simplify the fabrication process, these crosslinkers are often added to the film-forming inks before processing. We previously

applied this method to the inkjet printing of water-resistant PEDOT:PSS layers for OECT applications.[27] Although the addition of crosslinkers simplifies the process, it can induce chemical reactions that destabilize the solution, resulting in aggregate formation or phase separation. Consequently, the use of a crosslinker is beneficial for the facile formation of a stable film; however, the stability of the ink must be monitored.

--<<Figure 1>>--

An alternative approach is to perform physical crosslinking process after the film has formed by removing the excess PSS from the film. In typical commercial PEDOT:PSS dispersions (**Figure 1**) such as Clevios PH 1000, the ratio of PSS to PEDOT far exceeds that of the hole dopant to PEDOT, which stabilizes the colloidal particles. The films produced from these dispersions are soluble in water; however, they can be stabilized by soaking in agents such as ionic liquids[28,29] and concentrated H_2SO_4[30,31] to remove the excess PSS. In a previous study, we developed a method to obtain self-standing thick PEDOT:PSS films using a gel-film formation process with ethanol soaking.[32,33] Although this approach produced self-standing films with micrometer thicknesses, its application in a thin-film regime has not been tested.

This study presents a crosslinker-free fabrication of water-resistant PEDOT:PSS-based films. To meet the growing demand for bioelectronic applications, we focused on three aspects: (1) films several tens of nanometers in thickness, (2) film formation on non-planer-shaped substrates, and (3) an annealing-free process under ambient conditions. Processes that meet these criteria will enable the facile coating of implantable bioelectronic devices such as

needle-shaped electrophysiological probes. Therefore, we employed a dip-coating process to coat differently shaped substrates other than plates. Although dip coating with PEDOT:PSS has been previously reported,[34-37] these studies did not examine the water resistance of the resulting films. We expanded our previously reported gel-film formation process[32,33] to dip-coated PEDOT:PSS films. The resulting PEDOT:PSS films were sequentially immersed in ethanol and water, and their properties were examined. Combined with chemical modification of the substrates to ensure good adhesion, the sequential dipping process afforded water resistance to the films. Spectroscopic and microscopic analyses confirmed that the removal of excess PSS in the dip-coated films proceeded in two stages during each immersion process. In addition, three-dimensional (3D) printed objects were coated to demonstrate conductive coatings on non-planar-shaped substrates. This study proposes a facile and generic methodology to obtain mixed-conductor films on digitally printed objects.

2. Results and Discussion

--<<Figure 2>>--

Figure 2(a) shows photographs of the PEDOT:PSS-coated glass substrates after the three sequential immersion processes of dip coating with PEDOT:PSS, soaking in ethanol, and soaking in water. During the surface modification process, the GOPS concentration was varied between 0.1 and 1 vol%. Delamination was observed on samples modified with 0.1–0.5% GOPS; however, the film on samples modified with 1.0% GOPS remained intact. Nevertheless, the film retained its shape without dissolving during the water-soaking process, indicating that the ethanol-soaking process afforded water resistance to the film itself, although it did not facilitate adhesion to the glass substrate. X-ray reflectometry (XRR) was used to estimate the thickness and density of the GOPS layers on GOPS-modified substrates with low (0.1%) and high (1.0%) GOPS concentrations (**Figure 2**(b)). Fitting the data to a three-box model (substrate/native oxide/GOPS) gives the electron density profiles shown in **Figure 2**(c), which indicated that the thickness of the GOPS on the high concentration-modified surface was significantly greater than that on the low-concentration-modified surface.[38 The profiles of the interface ($\rho/\rho_{Si} = 0.56$) and tail regions ($\rho/\rho_{Si} \sim 0.4$) of the sample treated with the 0.1% solution were consistent with those in a previous report on a self-assembled monolayer (SAM) of GOPS.[39] In comparison, the 1.0% solution-treated sample exhibited a plateau at a lower electron density ($\rho/\rho_{Si} = 0.38$), corresponding to a GOPS layer with low molecular density. The GOPS layer in the 1.0% solution-treated sample exhibited a sparse multilayered structure, whereas a rough monolayer (or quasi monolayer) was observed for the sample treated with 0.1% GOPS solution.[40] Kramer *et al.* reported

that the adhesion energy of rough-monolayer GOPS was lower than that of spin-coated thick GOPS layers,[41] and the observations of the 0.1% solution treated-sample appeared to correspond to this case. The optical image and XRR results indicated that a multilayered GOPS layer was required to stabilize the PEDOT:PSS film during the water-soaking process. These results showed that the sequential-soaking process afforded water-resistant PEDOT:PSS films without the addition of crosslinkers to the coating ink or using thermal annealing processes.

--<<Figure 3>>--

Figure 3(a–c) shows atomic force microscopy (AFM) topographic images of the PEDOT:PSS films after each process. The surface of the dip-coated film (Figure 3(a)) exhibited a moderately flat surface with a root-mean-square roughness (RMS) of 3.8 nm. The roughness increased to 4.2 nm after the ethanol-soaking process owing to the formation of aggregated objects on the surface. After soaking in water, the surface was flat and undamaged (RMS: 2.4 nm). Other than the aggregates observed in the AFM image after ethanol and water soaking, the surfaces exhibited similar features and fibril-like textures to those reported in previous studies on spin- and blade-coated PEDOT:PSS films.[42] This indicated that water soaking primarily affected the aggregated objects. The film thickness of each sample was estimated at the height of the scratched gap, and indicated a significant decrease from 97 to 71 nm after the ethanol-soaking process. The film thickness decreased slightly to 61 nm during the subsequent water soaking (Figure 3(d)). These results indicated that ethanol soaking removed most of the eluted materials, and that the surface aggregated objects were removed during the water-soaking process.

--<<Figure 4>>--

--<<Table 1>>--

Figure 4 shows the spectroscopic investigations of the PEDOT:PSS films at each step of the process. Ultraviolet–visible–near infrared (UV-vis-NIR) spectra (**Figure 4**(a)) were used to determine the elution of PSS, which has an absorption band at 224 nm.[43] The intensity of this peak decreased by 39% after the ethanol-soaking process, with only a slight further change (45% reduction from the as-coated film) during the water-soaking process. This indicated that the PSS is largely eluted from the film during the ethanol soaking. **Figure 4**(b) shows the XPS spectra of the S2p region. According to previous reports, the peaks at 171 and 166 eV are attributed to SO_3 groups in PSS and PEDOT, respectively.[21,44] Note that the marginal part of SO_3 signal is from DBSA, yet the majority is from PSS, considering the amount added (1:17 based on weight ratio between DBSA and PEDOT:PSS). The spectral change corresponded to the reduction of the PSS moiety, which agreed well with the UV-vis-NIR results. **Figure 4**(c) shows a summary of the PSS concentration changes during the ethanol- and water-soaking processes. Notably, the spectral changes during water soaking were less significant in the UV-vis spectra than in the XPS spectra. This was because XPS can only detect within ca. 10 nm below the surface of the sample, and the PSS elution from the bulk was minimal compared to that from the film surface during the water soaking; **Figure 4**(d) shows the conductivity σ of the film estimated using the four-terminal measurement probe technique. The conductivity was enhanced after ethanol soaking and was retained during the water-soaking process. **Table 1** summarizes[45-49] and compares the conductivity of the PEDOT:PSS film fabricated in this study with those of other PEDOT-

based films fabricated using various techniques. Notably, the value observed in this study (500 S cm^{-1}) is the highest among the reported values for non-annealed films. The high conductivity indicated that PSS elution from the film bulk was dominant during the ethanol-soaking process, which purified the PEDOT-rich domain and increased the conductivity. In contrast, although the water-soaking process did not significantly impact the composition of the film bulk, it did remove the aggregates from the film surface. Based on the microscopic and spectroscopic data, the proposed mechanism for the formation of a water-resistant PEDOT:PSS film is illustrated in **Figure 4**(e). During the dip-coating step, a PEDOT:PSS film formed on the substrates and was adhered to the substrate by GOPS via the chemical reaction between PSS and GOPS, as mentioned in previous reports.[21] The subsequent ethanol-soaking process removed the excess PSS from the film bulk and the remaining PSS aggregated on the surface of the film, as observed in the AFM images. The elution of excess PSS continued until the PEDOT to PSS ratio was 1:1.5, at which point all PSS that was not bound to the PEDOT had been removed. This was confirmed by the decrease in the absorbance at 224 nm (Figure 4(a)) because a 39% reduction in absorbance corresponds to PEDOT:PSS = 1:1.5; this was based on an initial ratio of Clevios PH1000 PEDOT:PSS = 1:2.5.[50,51] The subsequent water-soaking process removed the aggregated PSS from the film surface and had minimal impact on the bulk, as indicated by the minor changes in the UV-vis spectra. Throughout the process, removing excess PSS from the film bulk enhanced the resistance of the film to water. The moderately slow elution of PSS during ethanol soaking and the anchoring effect of GOPS prevented the dissolution and delamination of the entire film.

--<<Figure 5>>--

To demonstrate its versatility, the developed technique was used to coat the surfaces of non-planer objects, including 3D-printed objects. **Figure 5**(a) shows a coated glass bar with a diameter of 5 mm after GOPS modification, similar to the glass slides shown in **Figure 2**(a). The surface was uniformly coated, and resistance measurement with Kelvin clips was used to confirm a high conductivity of $RL^{-1} = 2.4\ \Omega\ mm^{-1}$. This confirms that the technique can be applied to non-planar surfaces in lieu of spin-coating and inkjet printing techniques. **Figure 5**(b) and (c) shows PEDOT:PSS-coated poly(lactic acid) (PLA) and thermoplastic urethane (TPU) objects printed using a commercially available 3D printer. The complicated surfaces were successfully coated with PEDOT:PSS, which imparted conductivity to the surfaces. In addition, the surface of the object can be modified with GOPS using a vapor-phase treatment under reduced pressure. However, GOPS modification of the sample is not mandatory and a stable coating can be obtained using only oxygen plasma treatment, owing to the presumed formation of polar groups on the surface of the PLA.[52] The stability and conductivity of the PEDOT:PSS coating was tested via bending tests on the coated TPU sheet, as shown in **Figure 5**(c). **Figure 5** (d) shows the resistance change over the uniaxial bending to $L/L_0 = 0.2$, where L and L_0 indicate the edge-to-edge length of the initial and bent objects, respectively. A slight increase in resistivity was observed upon bending; however, the conductivity was retained during the bending process. **Figure 5**(e) shows the resistance change under repeated bending to $L/L_0 = 0.2$. The change in resistance upon bending was less than 5%, indicating the stable coating and adhesion of the PEDOT:PSS layer to the TPU object. These observations confirmed the conductivity and durability of the PEDOT:PSS-coated layer.

--<<Figure 6>>--

The dip-coated PEDOT:PSS films were used to fabricate an OECT device on a non-planar surface. **Figure 6** (a) shows a photograph of an OECT device fabricated in a polypropylene pipette tip with a source-to-drain gap of ca. 1 mm. The device exhibited depression mode operation in phosphate-buffered saline (PBS) (**Figure 6**(b) and (c)). Similar results have been reported for OECT devices on flat substrates,[12,13] a flexible substrate,[53] and a fully digitally printed device.[27] This confirmed that the PEDOT:PSS films proposed here can serve as a channel layer in OECT devices with non-planar surfaces. In addition, the OECT was applied as a neuromorphic device, as shown in **Figure 6**(d) –(f), using paired-pulse depression (PPD) and adaptation tests.[54,55] In the PPD test, the drain current exhibited a millisecond-long spike that corresponded to the signal-of-interest, followed by a relaxation to the steady-state on the gate voltage input. Note that the spike is from gate current as we previously pointed out in another paper.[55] The depression degree $1 - A_2/A_1$ was estimated based on the amplitudes of the spikes on the first and second pulses A_1 and A_2 as a function of the pulse interval Δt (**Figure 6**(e)). The curves exhibited typical PPD behavior, with the degree of depression decreasing as the pulse interval increased. The retention time was estimated by fitting the curves to an exponential function and the time constant for information retention τ_{PPD} was determined to be 178 ms for this device. Based on the time constant, an adaptation test was performed using Δt = 100, 200, and 500 ms. **Figure 6**(f) shows the resulting adaptations in the OECT drain current. The drain current response to the pulse train adapted to a steady-state value when $\Delta t \lesssim \tau_{PPD}$. This was because the injected cations from the PBS buffer had insufficient time to return to the electrolyte before a new pulse was injected. In contrast, the long interval of Δt = 500 ms was sufficient for the cations

to return to solution.[54,55] This result is relevant to our previous report on OECT devices prepared using fully digital printing technologies.[27] Consequently, the proposed process can be used to prepare OECT devices similar to those prepared using conventional spin-coating and digital-printing techniques.

3. Conclusions

We developed a facile and generic method to fabricate water-resistant PEDOT:PSS films on non-planar surfaces without the use of chemical crosslinking agents. The analysis highlighted two critical points in the proposed process: (1) elution of excess PSS from the film bulk using ethanol soaking to stabilize the film prior to the water-soaking process, and (2) coating non-planar surfaces, including 3D printed objects, with conductive coatings under ambient conditions. Although further studies are required to elucidate the crystal structure and molecular alignment of the materials, these findings can potentially facilitate the efficient prototyping and production of implantable devices, including OECTs, bioelectronic probes, and bioelectrodes, which can advance the emerging field of organic bioelectronic devices. In particular, the combination of this technique with digital printing technology will enable not only advanced facilities but also small-scale digital fabrication workshops to access cutting-edge conductive polymer technology.

4. Materials and Methods

4.1 Preparation of PEDOT:PSS Ink

The PEDOT:PSS solution was prepared according to a previously reported method.[54,55] PEDOT:PSS (Clevios, pH 1000) and ethylene glycol (EG) (FUJIFILM Wako Pure Chemical Co.) were used as the polar solvents, and dodecylbenzenesulfonic acid (DBSA) (Tokyo Kasei) as the surfactant; the mixture was sonicated for 15 min.

4.2 Preparation of Glass Substrates and 3D-Printed Objects

Glass, quartz, and silicon substrates were cleaned in an ultrasonic bath with acetone, isopropyl alcohol, and deionized (DI) water, and treated with UV–ozone for 30 min. The substrates were immersed in an anhydrous toluene solution of GOPS (Tokyo Kasei) at concentrations of 0.1–1 vol% and stored overnight in a desiccator. The treated substrates were thoroughly rinsed with toluene and dried under a stream of nitrogen gas. The 3D-printed objects were prepared using commercially available printers (Dreamer and Finder 3; Flashforge) with thermal extruders. PLA and TPU filaments (Flashforge) were used for printing. The printed objects were treated with an oxygen plasma using a plasma etcher (SEDE-MN; Meiwafosis) before coating.

4.3 Dip Coating and Sequential Immersion

The substrates were dip coated with the PEDOT:PSS ink at room temperature with a dip coater (ND-0407-S4; SDI). The coating was performed at a drawing speed of 50 μm s^{-1} and the coated substrates were dried in a desiccator overnight. The coated objects were immersed in ethanol for 3 h and then in water overnight. The final sample was dried under a stream of nitrogen gas.

4.4 Analysis

The surface morphology and thickness were observed using an AFM (SPA400; Seiko Instruments) with Si cantilevers (SI-DF20, 15 N m^{-1}; Hitachi) in dynamic mode. XRR measurements were performed using an X-ray diffractometer system (SmartLab; Rigaku). CuKα (λ = 0.154 nm) X-rays were irradiated on the sample and detected by a scintillation counter (SC-70; Rigaku) over a $2\theta/\omega$ scan. The XRR data were analyzed using the GenX software package.[38] UV-vis measurements were performed using a spectrophotometer (V-670; JASCO) on quartz substrates. XPS measurements were performed using an XPS instrument (PHI 5600; PerkinElmer). The electrical resistance of the samples was measured

on glass substrates via the four-probe method using an in-house experimental setup.[32,33] Conductivity measurements of the 3D-printed objects were performed using a resistance meter (3541; HIOKI) equipped with Kelvin clips.

4.5 Pipette-Tip OECT Device Fabrication

A polypropylene pipette tip (200 μL; AS ONE Corporation) was masked using masking tape, treated with oxygen plasma, and coated with a dispersion of gold nanoparticles (Dry Cure Au-J, C-INK), followed by thermal treatment at 90 °C to fabricate the source and drain electrodes. The tip was coated with PEDOT:PSS and treated according to the previously described procedure. The coated tip was immersed in PBS buffer together with an Ag/AgCl gate electrode (EP2; World Precision Instruments). Electrical measurements were performed inside a Faraday cage, and source measure units (Keysight 2450 and 2451) were used to measure the device properties.

FIGURES

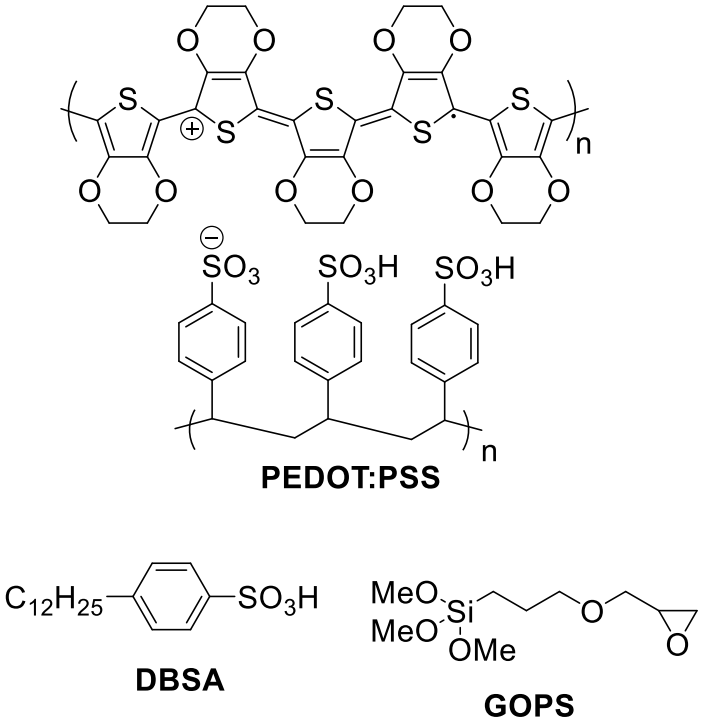

Figure 1. Chemical structures of the materials used in this study.

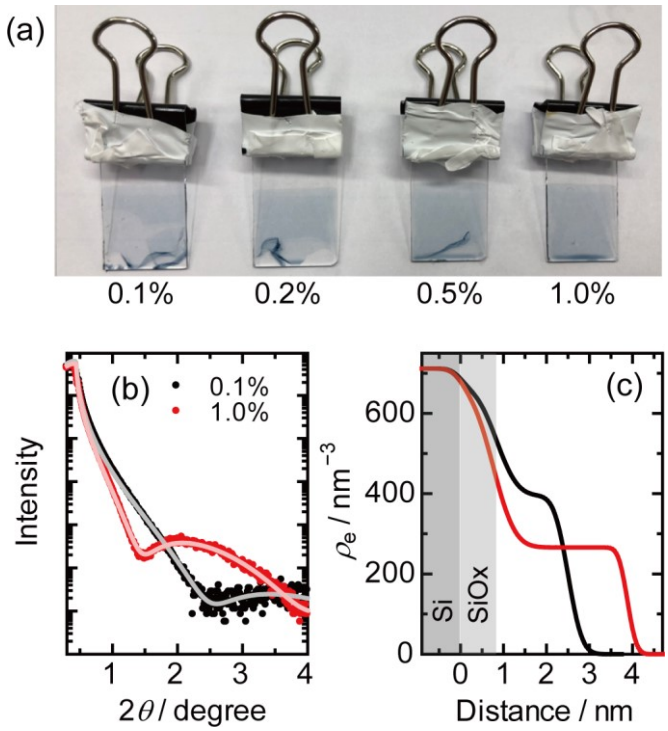

Figure 2. (a) Photographs of PEDOT:PSS films coated on GOPS-modified glass substrates (15 × 25 mm). The numbers below each image indicate the GOPS concentration used in the surface modification process. (b) XRR profiles and (c) corresponding fitting results of GOPS-modified Si wafers with various GOPS concentrations. In panel (c), solid lines indicate model fitting, and solid gray regions correspond to the substrate and native oxide layer.

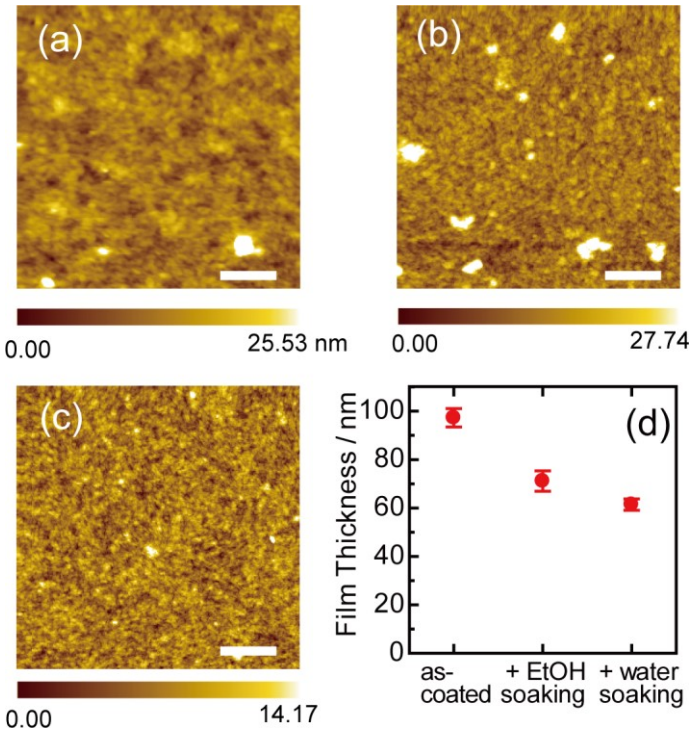

Figure 3. AFM topographic images of PEDOT:PSS films (a) after dip coating, (b) after ethanol soaking, and (c) after water soaking. The scale bars indicate a length of 1 μm. (d) Film thickness determined from AFM measurements after each process. The error bars indicate RMS roughness.

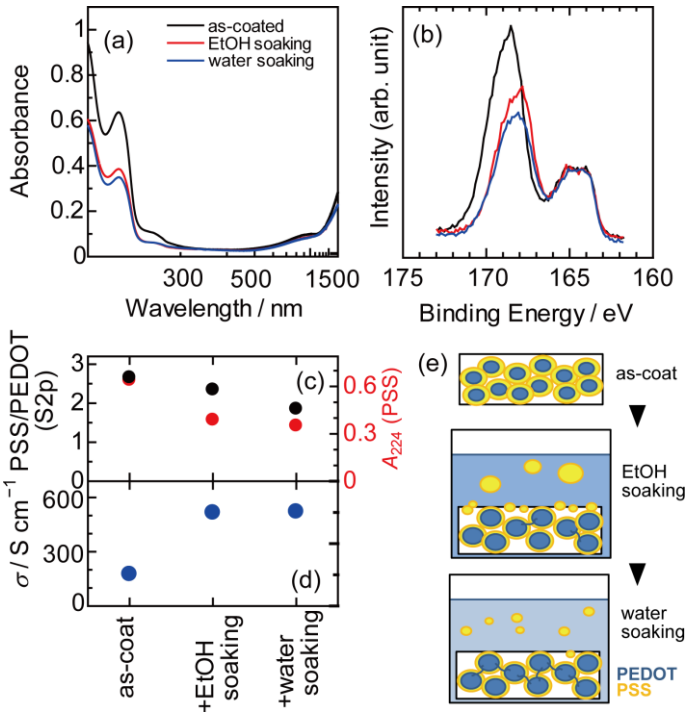

Figure 4. (a) UV-vis and (b) XPS (S2p) spectra of PEDOT:PSS films (black) after dip coating, (red) after ethanol soaking, and (blue) after water soaking. (c) Plots of (black) the ratio of the XPS signal area corresponding to PSS and PEDOT in the S2p region, (red) absorbance at 224 nm originating from PSS, and (d) conductivity after each process. (e) Proposed mechanism of water-resistant PEDOT:PSS film formation via sequential dipping processes; removal of the excess PSS (i) from the film bulk and (ii) from the surface of the film.

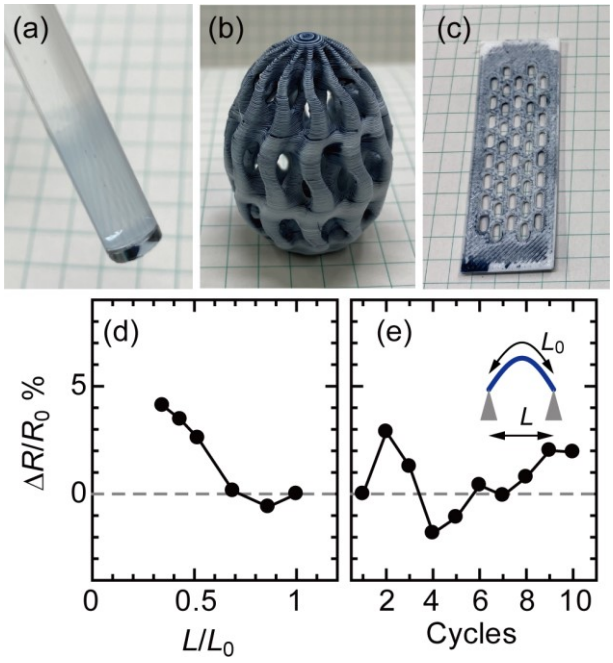

Figure 5. Photographs of non-planar objects coated with PEDOT:PSS at a drawing speed of 50 μm s^{-1} (a): glass bar, (b): PLA; (c): TPU). Resistivity change during bending tests over (d) bending radius L/L_0, and (e) cycles of bending to L/L_0 = 0.2. (Object (b) was created by Thingiverse user DaveMakesStuff, and is licensed under cc-nc-sa: https://www.thingiverse.com/thing:5945616)

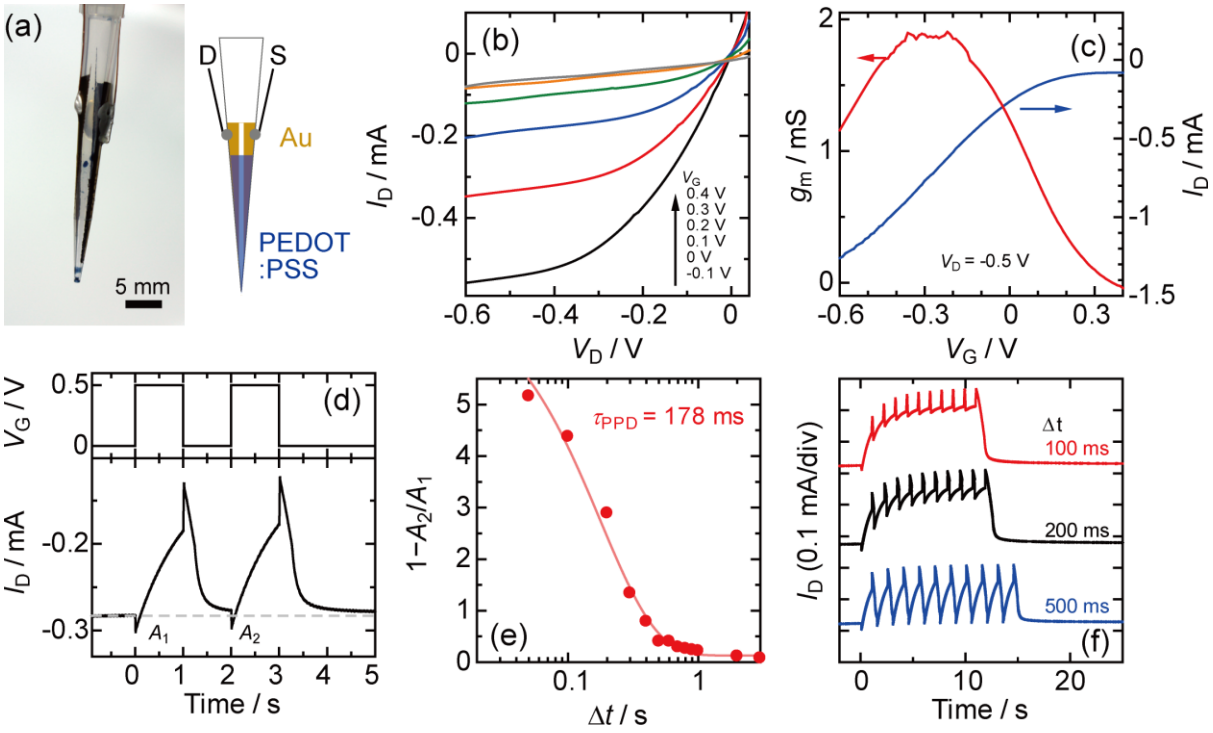

Figure 6. (a) Photograph and diagram of an OECT device in pipette tip. (b) Output and (c) transfer curves of the device operated in PBS buffer with an Ag/AgCl pallet as the gate electrode. (d) Paired-pulse-depression (PPD) in OECTs; applied voltage stimulus at the gate with pulse width amplitude V_G = +0.5 V, period t_p = 1 s, and pulse interval Δt = 1 s led to transient drain currents (I_D). The drain voltage (V_D) was −0.5 V. (e) Depression in I_D amplitude from baseline as a function of pulse interval Δt for OECTs. (f) Adaptation in OECTs with various pulse intervals. A train of gate pulses was applied to the device, and the I_D was measured as a function of time.

Table 1. Conductivities of PEDOT:PSS materials prepared via various methods.

Study	Method	Annealing	Conductivity / S cm^{-1}
This Work	Dip Coating	N	522
Liu *et al.*[45]	Cast with DMSO	N	298
Okuzaki *et al.*[46]	Wet spinning and EG treatment	N	467
Fall *et al.*[47]	Wet spinning with CNF and EG treatment	N	154
Kim *et al.*[48]	Spin Coating	Y	634
	+ EG soaking	Y	1330
Wei *et al.*[49]	Spin Coating	Y	830

Conflict of Interest

The authors declare no conflict of interest.

Acknowledgments

The authors thank Ms. Sayaka Ogawa, IMRAM, Tohoku University, for XPS measurements, and Innovation Plaza, School of Engineering, Tohoku University, for the 3D printing. This work was supported by JSPS KAKENHI Grant Number JP21H01992 and the Amano Institute of Technology.

Data Availability Statement

The data that support the findings of this study are available from the corresponding author upon reasonable request.

REFERENCES

[1] B. D. Paulsen, K. Tybrandt, E. Stavrinidou, J. Rivnay, *Nat. Mater.* **2019**, *19*, 13.

[2] N. A. Kukhta, A. Marks, C. K. Luscombe, *Chem. Rev.* **2022**, *122*, 4325.

[3] Someya, T.; Bao, Z.; Malliaras, G. G. The Rise of Plastic Bioelectronics. *Nature* **2016**, *540* (7633), 379–385.

[4] M. Sophocleous, L. Contat-Rodrigo, E. Garcia-Breijo, J. Georgiou, *IEEE Sens. J.* **2021**, *21*, 3977.

[5] C. Wang, T. Yokota, T. Someya, *Chem. Rev.* **2021**, *121*, 2109.

[6] F. Torricelli, D. Z. Adrahtas, Z. Bao, M. Berggren, F. Biscarini, A. Bonfiglio, C. A. Bortolotti, C. D. Frisbie, E. Macchia, G. G. Malliaras, I. McCulloch, M. Moser, T. Q. Nguyen, R. M. Owens, A. Salleo, A. Spanu, L. Torsi, *Nat. Rev. Methods Prim.* **2021**, *1*, 66.

[7] A. Marks, S. Griggs, N. Gasparini, M. Moser, A. Marks, S. Griggs, M. Moser, N. Gasparini, *Adv. Mater. Interfaces* **2022**, *9*, 2102039.

[8] L. D. Garma, L. M. Ferrari, P. Scognamiglio, F. Greco, F. Santoro, *Lab Chip* **2019**, *19*, 3776.

[9] M. L. Picchio, A. Gallastegui, N. Casado, N. Lopez-larrea, B. Marchiori, I. Agua, M. Criado-gonzalez, D. Mantione, R. J. Minari, D. Mecerreyes, N. Lopez-Larrea, B. Marchiori, I. del Agua, M. Criado-Gonzalez, D. Mantione, R. J. Minari, D. Mecerreyes, N. Lopez-larrea, B. Marchiori, I. Agua, M. Criado-gonzalez, D. Mantione, R. J. Minari, D. Mecerreyes, N. Lopez-Larrea, B. Marchiori, I. del Agua, M. Criado-Gonzalez, D. Mantione, R. J. Minari, D. Mecerreyes, *Adv. Mater. Technol.* **2022**, *2101680*, 2101680.

[10] N. Casado, S. Zendegi, L. C. Tomé, S. Velasco-Bosom, A. Aguzin, M. Picchio, M. Criado-Gonzalez, G. G. Malliaras, M. Forsyth, D. Mecerreyes, *J. Mater. Chem. C* **2022**, *10*, 15186.

[11] N. Lopez-Larrea, M. Criado-Gonzalez, A. Dominguez-Alfaro, N. Alegret, I. Del Agua, B. Marchiori, D. Mecerreyes, *ACS Appl. Polym. Mater.* **2022**, *4*, 6749.

[12] J. Rivnay, S. Inal, A. Salleo, R. M. Owens, M. Berggren, G. G. Malliaras, *Nat. Rev. Mater.* **2018**, *3*, 17086.

[13] S. Yamamoto, *Polym. Int.* **2023**, *72*, 609.

[14] W. Lee, D. Kim, J. Rivnay, N. Matsuhisa, T. Lonjaret, T. Yokota, H. Yawo, M. Sekino, G. G. Malliaras, T. Someya, *Adv. Mater.* **2016**, 9722.

[15] C. Cea, G. D. Spyropoulos, P. Jastrzebska-Perfect, J. J. Ferrero, J. N. Gelinas, D. Khodagholy, *Nat. Mater.* **2020**, *19*, 679.

[16] S. Han, A. G. Polyravas, S. Wustoni, S. Inal, G. G. Malliaras, *Adv. Mater. Technol.* **2021**, *6*, 2100763.

[17] X. Crispin, S. Marciniak, W. Osikowicz, G. Zotti, A. W. Denier Van Der Gon, F. Louwet, M. Fahlman, L. Groenendaal, F. De Schryver, W. R. Salaneck, *J. Polym. Sci. Part B Polym. Phys.* **2003**, *41*, 2561.

[18] J. Huang, P. F. Miller, J. C. De Mello, A. J. De Mello, D. D. C. Bradley, *Synth. Met.* **2003**, *139*, 569.

[19] H. Yan, S. Arima, Y. Mori, T. Kagata, H. Sato, H. Okuzaki, *Thin Solid Films* **2009**, *517*, 3299.

[20] D. Khodagholy, T. Doublet, M. Gurfi nkel, P. Quilichini, E. Ismailova, P. Leleux, T. Herve, S. Sanaur, C. Bernard, G. G. Malliaras, D. Khodagholy, T. Doublet, M. Gurfi nkel, E. Ismailova, P. Leleux, S. Sanaur, G. G. Malliaras, P. Quilichini, C. Bernard, T. Herve, *Adv. Mater.* **2011**, *23*, H268.

[21] A. Håkansson, S. Han, S. Wang, J. Lu, S. Braun, M. Fahlman, M. Berggren, X. Crispin, S. Fabiano, *J. Polym. Sci. Part B Polym. Phys.* **2017**, *55*, 814.

[22] D. Mantione, I. Del Agua, W. Schaafsma, M. Elmahmoudy, I. Uguz, A. Sanchez-Sanchez, H. Sardon, B. Castro, G. G. Malliaras, D. Mecerreyes, *ACS Appl. Mater. Interfaces* **2017**, *9*, 18254.

[23] N. Lopez-Larrea, M. Criado-Gonzalez, A. Dominguez-Alfaro, N. Alegret, I. Del Agua, B. Marchiori, D. Mecerreyes, *ACS Appl. Polym. Mater.* **2022**, *4*, 6749.

[24] M. Solazzo, K. Krukiewicz, A. Zhussupbekova, K. Fleischer, M. J. Biggs, M. G. Monaghan, *J. Mater. Chem. B* **2019**, *7*, 4811.

[25] G. Polino, C. Lubrano, P. Scognamiglio, V. Mollo, S. De Martino, G. Ciccone, L. Matino, A. Langella, P. Netti, A. Di Carlo, F. Brunetti, F. Santoro, *Flex. Print. Electron.* **2020**, *5*, 014012.

[26] S. Kindaichi, R. Matsubara, A. Kubono, S. Yamamoto, M. Mitsuishi, *ChemRxiv* https://doi.org/10.26434/chemrxiv-2023-ztqm (Posted on Apr 25, 2023).

[27] T. N. Mangoma, S. Yamamoto, G. G. Malliaras, R. Daly, *Adv. Mater. Technol.* **2020**, 2000798.

[28] S. Kee, N. Kim, B. S. Kim, S. Park, Y. H. Jang, S. H. Lee, J. J. J. Kim, J. J. J. Kim, S. Kwon, K. Lee, *Adv. Mater.* **2016**, *28*, 8625.

[29] A. De Izarra, C. Choi, Y. H. Jang, Y. Lansac, *J. Phys. Chem. B* **2021**, *125*, 1916.

[30] S. M. Kim, C. H. Kim, Y. Kim, N. Kim, W. J. Lee, E. H. Lee, D. Kim, S. Park, K. Lee, J. Rivnay, M. H. Yoon, *Nat. Commun.* **2018**, *9*, 3858.

[31] Y. Li, S. Zhang, N. Hamad, K. Kim, L. Liu, M. Lerond, F. Cicoira, *Macromol. Biosci.* **2020**, *20*, 2000146.

[32] R. Maeda, H. Kawakami, Y. Shinohara, I. Kanazawa, M. Mitsuishi, *Mater. Lett.* **2019**, *251*, 169.

[33] R. Maeda, Y. Shinohara, H. Kawakami, Y. Isoda, I. Kanazawa, M. Mitsuishi, *Nanotechnology* **2021**, *32*, 135403.

[34] Z. Hu, J. Zhang, S. Xiong, Y. Zhao, *Org. Electron.* **2012**, *13*, 142.

[35] L. Huang, Z. Hu, K. Zhang, P. Chen, Y. Zhu, *Thin Solid Films* **2015**, *578*, 161.

[36] Y. Ding, J. Yang, C. R. Tolle, Z. Zhu, *ACS Appl. Mater. Interfaces* **2018**, *10*, 16077.

[37] H. Takise, T. Shintani, M. Suzuki, T. Takahashi, S. Aoyagi, *Electron. Commun. Japan* **2020**, *103*, 46.

[38] M. Bjorck, G. Andersson, *J. Appl. Crystallogr.* **2007**, *40*, 1174.

[39] I. Luzinov, D. Julthongpiput, A. Liebmann-Vinson, T. Cregger, M. D. Foster, V. V. Tsukruk, *Langmuir* **2000**, *16*, 504.

[40] V. V. Tsukruk, I. Luzinov, D. Julthongpiput, *Langmuir* **1999**, *15*, 3029.

[41] J. J. Benkoski, E. J. Kramer, H. Yim, M. S. Kent, J. Hall, *Langmuir* **2004**, *20*, 3246.

[42] B. J. Worfolk, S. C. Andrews, S. Park, J. Reinspach, N. Liu, M. F. Toney, S. C. B. Mannsfeld, Z. Bao, *Proc. Natl. Acad. Sci. U. S. A.* **2015**, *112*, 14138.

[43] C. De Saint-Aubin, J. Hemmerlé, F. Boulmedais, M. F. Vallat, M. Nardin, P. Schaaf, *Langmuir* **2012**, *28*, 8681.

[44] G. Zotti, S. Zecchin, G. Schiavon, F. Louwet, L. Groenendaal, X. Crispin, W. Osikowicz, W. Salaneck, M. Fahlman, *Macromolecules* **2003**, *36*, 3337.

[45] C. Liu, B. Lu, J. Yan, J. Xu, R. Yue, Z. Zhu, S. Zhou, X. Hu, Z. Zhang, P. Chen, *Synth. Met.* **2010**, *160*, 2481.

[46] H. Okuzaki, Y. Harashina, H. Yan, *Eur. Polym. J.* **2009**, *45*, 256.

[47] A. B. Fall, F. Hagel, J. Edberg, A. Malti, P. A. Larsson, L. Wågberg, H. Granberg, K. M. O. Håkansson, *ACS Appl. Polym. Mater.* **2022**, *4*, 4119.

[48] Y. H. Kim, C. Sachse, M. L. Machala, C. May, L. Müller-Meskamp, K. Leo, *Adv. Funct. Mater.* **2011**, *21*, 1076.

[49] Q. Wei, M. Mukaida, Y. Naitoh, T. Ishida, *Adv. Mater.* **2013**, *25*, 2831.

[50] A. Anand, J. P. Madalaimuthu, M. Schaal, F. Otto, M. Gruenewald, S. Alam, T. Fritz, U. S. Schubert, H. Hoppe, *ACS Appl. Electron. Mater.* **2021**, *3*, 929.

[51] Z. T. Gebremichael, C. Ugokwe, S. Alam, S. Stumpf, M. Diegel, U. S. Schubert, H. Hoppe, *RSC Adv.* **2022**, *12*, 25593.

[52] A. Jordá-Vilaplana, V. Fombuena, D. García-García, M. D. Samper, L. Sánchez-Nácher, *Eur. Polym. J.* **2014**, *58*, 23.

[53] S. Yamamoto, H. Kai, *Adv. Mater. Interfaces* **2022**, *9*, 2201736.

[54] S. Yamamoto, G. G. Malliaras, *ACS Appl. Electron. Mater.* **2020**, *2*, 2224.

[55] S. Yamamoto, A. G. Polyravas, S. Han, G. G. Malliaras, *Adv. Electron. Mater.* **2022**, *8*, 2101186.